Magazine of Civil Engineering

ISSN 2712-8172

journal homepage: http://engstroy.spbstu.ru/

Research article
UDC 624
DOI: 10.34910/MCE.112.11

Structural performance of corroded RC beams without shear reinforcement

N.T. Nguyen ✉, ***T.K. Nguyen***, ***H.G. Nguyen***

Hanoi University of Civil Engineering, Hanoi city, Vietnam

✉ *tannn@huce.edu.vn*

Keywords: reinforced concrete beams, reinforcement corrosion, shear strength, modeling, finite element method

Abstract. In this paper, a total of eight medium-scale RC beams with the dimensions of 150×200×1100 mm were fabricated without shear reinforcements. These beams were subjected to an accelerated corrosion test and then to a four-point loading shear test. The key test variables were various degrees of corrosion introduced in the tension reinforcements (0 %, 3.13 %, 4.11 %, and 4.93 % by mass loss). Even though all tested beams collapsed in shear failure, corroded beams exposed to 3 % and 4 % corrosion degrees showed a clear upward trend of approximately 7 % of maximum capacity compared to control beams. In contrast, corroded beams having a 5 % corrosion degree showed a 10 % decrease in shear strength with distinguished cracking patterns and load-carrying mechanism because of the significant loss of bond strength due to corrosion. Furthermore, a finite element model (FEM) for the prediction of structural performance in tested beams was produced using DIANA software. This model was verified by the experimental results (e.g. load-deflection curves, cracking patterns) with good agreement. Lastly, the parametric study of different shear span-to-depth ratios was also conducted to examine the FEM capability in simulating different behavior associated with beam and tie-arched mechanisms.

Funding: The authors would like to thank the financial support from the National University of Civil Engineering (NUCE), Hanoi, Vietnam, under grant number 47-2021/KHXD.

Citation: Nguyen, N.T., Nguyen, T.K., Nguyen, H.G. Structural performance of corroded RC beams without shear reinforcement. Magazine of Civil Engineering. 2022. 112(4). Article No. 11211. DOI: 10.34910/MCE.112.11

1. Introduction

Steel reinforcement corrosion inflicts damage that induces a deterioration in the performance and significantly impairs the mechanical properties of RC structures. There should be attention paid to the fact that RC structures tend to be exposed to deteriorative agents throughout their service life. The residual strength and load-carrying mechanism of these structures must be calculated to effectively rehabilitate the degraded RC structures subjected to corrosion.

There are numerous comprehensive studies of experimental efforts assessing the flexural behavior of corroded RC structures. It has been generally accepted that the flexural capacity of corroded members is directly associated with the remaining sectional area of reinforcing rebars and that ductility is degraded by corrosion of longitudinal reinforcement [1–7]. Along with the majority of the previous studies that have investigated mainly the flexural behavior of corroded RC structures, more and more researchers focused on the shear strength of corroded beams [8–11], because the corrosion of reinforcement had altered the failure mode from bending for non-corroded beams to shear for corroded beams [5]. It means that the design of RC beams with a higher shear capacity to avoid such sudden failure is compulsory.

Recently, because of a large number of existing deteriorated structures, reliable methods that can evaluate the residual structural performance to facilitate repair and maintenance strategies are in great demand. Accurate performance evaluation of the deteriorated structures from the numerical analysis may allow the extension of service life and increase the safety level across a network of deteriorated structures [12]. Therefore, numerical approach researches from 2004 to 2020 [12–18] are necessary. However, comparatively less attention has been devoted to assessing the residual structural capacity of corroded RC beams without stirrups using the finite element method (FEM) [19, 20]. The study of Toongoenthong and Maekawa [19] on spatially localized cracking and pre-induced damage along with the longitudinal reinforcement of RC beam by simulating the corrosion effect has shown that corrosion cracking does not necessarily always bring a non-favorable effect on the structural behavior of corroded RC members because of the steel and concrete bond performance. With sufficient anchorage performance, the bond deterioration caused by corrosion cracks in the shear span may lead to tied-arch action with the increase of shear capacity. It shares the same agreement with the research work conducted by Han et al. [20], in which the tension reinforcement was properly anchored using the hook details: the RC beams constructed without stirrups subjected to less than 5 % corrosion degree showed about 40 % enhancement in shear resistance capacity due to the transfer mechanism shifting from beam action to tied-arch action, regardless of the reduction in bond performance.

Thus, the experimental and simplified modeling methodologies are addressed in this study, focusing on the bond behavior of corroded RC beams without stirrups. Corrosion-induced damages will be modeled by considering corrosion-induced cracking, changing the properties of concrete and steel, and modifying the bond between tension reinforcement and concrete. Thereafter, the FE model was validated by calibrating the test results obtained on a set of eight RC beams in an experimental program. The main parameters of the non-linear analysis consist of the relationship between load and mid-span deflection, the cracking patterns, and failure mode. Finally, a parametric study has been investigated and discussed to assess the effect of the shear span-to-depth ratio on the structural performance of corroded RC beams without stirrups.

2. Methods

2.1. Experimental method

The composition of the concrete used, consisting of Portland cement, river sand, crushed stone with a maximum diameter of 20 mm, and water, is presented in Table 1. The water-cement ratio is equal to 0.42. The compression test was performed on a sample group of three cubes with the dimensions of 150×150×150 mm at 28 days. The results show that the average concrete compressive strength is equivalent to 25.1 MPa, with a standard deviation of 0.4 MPa and a coefficient of variation of 1.5 % [21].

Table 1. Concrete mix.

Cement (kg)	Fine aggregates (kg)	Coarse aggregates (kg)	Water (liter)	W/C
439	622	1211	185	0.42

Ribbed steel rebars with a nominal diameter of 16 mm are longitudinal reinforcement inside the experimental beams. The tensile strengths of steel rebars were also calculated in the laboratory by the tension test, with the average yield tensile strength and ultimate tensile strength of 328.5 and 528.8 MPa, respectively. The length and the initial mass before corrosion have been weighted among all steel rebars. In this study, in order to investigate the influence of corroded tension reinforcement on the structural performance of the RC beams made without stirrups and to validate the finite element (FE) model, eight experimental beams with the dimensions of 150×200×1100 mm with a different configuration of steel corrosion degrees were tested under static loading. Each experimental beam was manufactured of concrete having the compressive strength of 25.1 MPa and two φ16 longitudinal steel rebars at the bottom layer as illustrated in Fig. 2(a) and without shear reinforcement (stirrups). The depth of the concrete cover is 40 mm from the bottom face of the beam.

Six beams were subjected to an accelerated corrosion test after 28 days of curing, as shown in Fig. 1. The steel rebars are wired to the power supplier's anode, while the cathode is connected to the copper rebar embedded in the 3.5 % sodium chloride solution. Only the experimental beams' bottom face is in contact with the solution. The solution depth is preserved at approximately 2 cm from the beam bottom. The steel rebars were not soaked in the solvent in order to protect exterior rebars from corrosion locally.

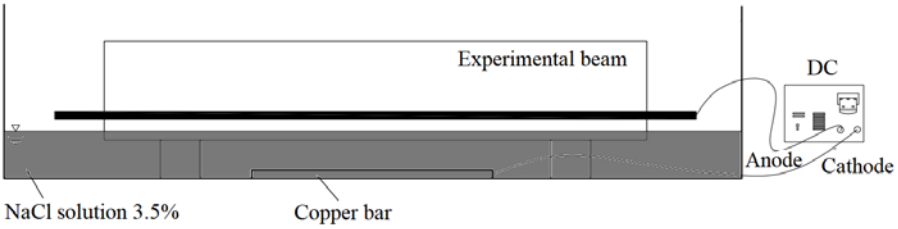

Figure 1. Detail of accelerated corrosion test.

For longitudinal reinforcement, the corrosion degree of the beam tested was determined based on the mass loss of the metal. The steel rebars were measured to assess the initial mass before doing the corrosion tests (m_o). The corroded reinforcements were separated from the beams for measurement after the corroded beams were exposed to monotonic loading for fracture. Firstly, the reinforcement was cleaned by a bristle brush to eliminate concrete adhering to the surface of the steel rebars. The reinforcement was then soaked in a 5 percent HCl solution for one day with 3.5 g hexamethylenetetramine and then cleaned to remove corrosion materials. The cleaning technique was also applied without corrosion to the non-corroded steel rebar. The procedure resulted in an insignificant loss of the control steel rebar. Therefore, to assess the remaining mass (m), the steel rebars were weighed. The corrosion degree of the reinforcement, noted c (%), is defined by Eq. (1), with m_o (g) being the steel mass before corrosion, m (g) being the steel mass after corrosion, and Δm (g) being the steel mass loss by corrosion:

$$c(\%) = \frac{m_o - m}{m_o} \times 100 = \frac{\Delta m}{m_o} \times 100. \quad (1)$$

Table 2. Determination of corrosion degrees of steel rebars.

Test group	Beam notation	Initial mass (g)	Remaining mass (g)	Mass loss (g)	Corrosion degree (%)	Average degree (%)
C0	C0-1	1987	1987	0	0	0
	C0-2	1956	1956	0	0	
C3	C3-1	1964	1909	55	3.16	3.13
	C3-2	1881	1822	59	3.10	
C4	C4-1	1993	1932	61	4.27	4.1
	C4-2	1950	1888	62	3.94	
C5	C5-1	1947	1865	82	4.99	4.93
	C5-2	1872	1797	75	4.87	

Table 2 shows the results of the determination of steel corrosion degree for all testing beams. For each corroded beam, the corrosion degree is the average value of the two corroded rebars at the bottom layer (φ16 steel rebars). The eight tested beams were divided into four groups named C0, C3, C4, and C5, respectively. Group C0 consisted of two control beams. Group C3, C4, and C5 had two corroded beams. Each experimental beam was designated with two numbers: the first number indicating the average degree of corrosion (0 %, 3.13 %, 4.1 %, and 4.93 %), whereas the second number stands for the numerical order of the beam.

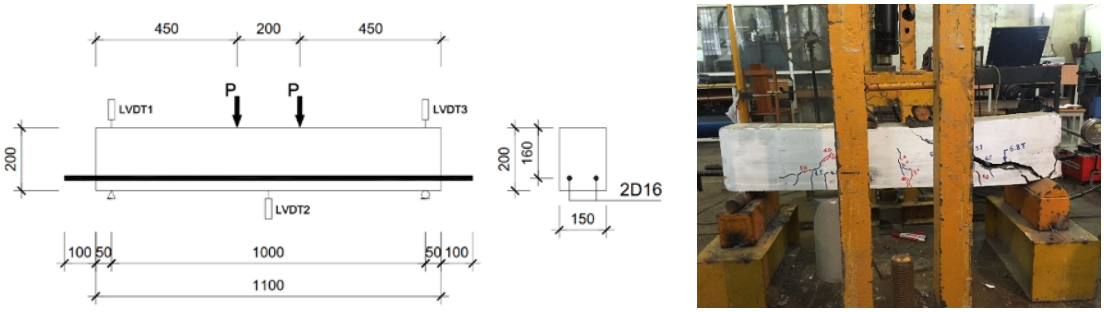

(a) **(b)**

Figure 2. Details of (a) test specimen and (b) four-point loading test.

In the four-point loading test setup, the shear span and effective depth were kept constant at 400 mm and 160 mm, respectively, in order to consider a shear span to depth ratio of 2.5 for all beams. The test specimens were subjected to monotonic loading, as illustrated in Fig. 2, to investigate the structural performance following the electrochemical accelerated corrosion of corroded beams and at least 28 days of curing with non-corroded beams. Over a clear span of 1100 mm, the beams were simply supported with two concentrated loads, which were both 400 mm apart from the supports R1 and R2. In order to calculate the vertical displacement of each beam measured, three Linear Variable Deformation Transducers (LVDTs) were mounted. The displacement transducer sets (LVDT1 and LVDT3) were used to calculate the displacement of the supports. In order to measure the displacement at the mid-span of the beam, the LVDT2 displacement transducer was used. A data-logger TDS-530 and a computer were connected to all displacement transducers to automatically collect measurement data to determine the relationship between the applied load and displacement.

2.2. Finite element modeling method

In this study, the numerical simulation was carried out in the DIANA software (version 10.3). In this three-dimensional analysis, the sensitivity of mesh was considered. It was verified in the study of Maekawa et al. in 1994 [22] that the tension-softening model used for concrete is independent of the element size. It should be noted that due to the heterogeneity in the concrete material, the minimum mesh size was taken as 20 mm (considering the maximum size of coarse aggregates). Therefore, the mesh size in the three-dimensional analysis can be sufficiently large without sacrificing accuracy [23]. The concrete model was based on a total strain fixed crack model. Firstly, the damage of concrete in the tested beam due to corrosion was modeled. The volumetric expansion from corrosion products induces internal pressure leading to the formation of concrete cover crack. In addition, the considerable effect of corrosion on the reduction of concrete compressive strength in the degraded area compared with the undamaged area was experimentally inspected in the study of Shayanfar et al. [24]. Therefore, the corrosion damage on the concrete cover is considered in the FE model by modifying the stress-strain relationship of the concrete as illustrated in Fig. 3(a), which was suggested by Coronelli and Gambarova [15] and validated in a numerical study of Lim et al. [25]. Whereas the behavior of concrete in compression is modeled using a parabolic curve in DIANA 9.1 User's manual [26]. The linear-elastic response up to 30% of the compressive strength of non-corroded concrete $\left(f_c'\right)$ is considered for stress levels, while the deterioration of the concrete compressive strength can be described by Eq. (2), with $f_{c,d}'$ being the compressive strength of the corroded concrete. The post-peak response of concrete in compression is modeled using compressive fracture energy, denoted G_C, based on the recommendations in studies of Nakamura and Higai [27]. While k' being the coefficient related to rebar roughness and diameter, for the case of medium-diameter ribbed rebars, a value k' = 0.1 has been proposed by Cape [28], ε_0 being the strain at the compressive strength f_c', and ε_1 being the average smeared tensile strain in the transverse direction:

$$f_{c,d}' = f_c' \Big/ \left[1 + k'\left(\varepsilon_1 / \varepsilon_0\right)\right]. \tag{2}$$

The strain ε_1 can be estimated by Eq. (3), with b_0 being the section width in the state without corrosion crack, b_f being the beam width expanded by corrosion cracking:

$$\varepsilon_1 = \left(b_f - b_0\right) \Big/ b_0, \tag{3}$$

$$b_f - b_0 = n_{bars} w_{cr}, \tag{4}$$

where n_{bars} is the number of rebars, and w_{cr} is the total crack width at a given corrosion degree. The total crack width w_{cr} can be calculated using Eq. (5) as recommended in the study of Molina et al. [29] in case of not having data from experiments:

$$w_{cr} = 2\left(v_{rs} - 1\right) X_d, \tag{5}$$

where v_{rs} is the ratio between the specific volumes of rust and steel that can be assumed to be 2. The depth of penetration attack X_d was determined by Eq. (6) as proposed in the study of Val [30], with

$i_{corr}\left(\mu A/cm^2\right)$ = 0.35 being the corrosion current density in the steel rebar and t (years) being the duration of corrosion:

$$X_d = 0.0116 i_{corr} t. \tag{6}$$

The tension softening behavior of concrete is represented using the non-linear curve of Hordijk et al., as described in DIANA 9.1 User's manual [26]. There, G_F is the tensile fracture energy, and h is the crack bandwidth taken as the square root of element area. All the input parameters, including G_F and tensile strength of concrete f_t' are obtained from CEB-FIP Mode Code [31] based on concrete compressive strength and maximum aggregate size. In this finite element simulation, the values of corroded compressive strength $f_{c,d}'$ are calculated using Eq. (2) and the reduced value of compressive fracture energy G_C is used for the concrete elements in order to model the effect of the loss of strength and ductility from the cracked concrete on the corroded tested beams.

Previous studies have indicated that corroded reinforcement strength and ductility are mainly affected by variability in the loss of steel cross-section across their lengths [32]. An alternative solution is proposed by modeling the corroded steel rebar over a length based on average cross-section loss along with empirical coefficients because of the difficulty in applying the real variability of steel corrosion in the numerical model.

In addition to the reduction attributed to the average cross-section, the use of empirical coefficients (whose values are lower than 1.0) is expected to account for the reduction in the strength and ductility of the corroded rebar due to the variable cross-sectional loss along the reinforcement length. The simplified bilinear constitutive stress-strain relationship of steel as shown in Fig. 3(b) is used without empirical coefficients, because the corrosion damage on the rebar is considered in the FE model by reducing the steel cross-sectional areas over the rebar length according to steel weight loss, where the post-yield module is presumed to be 1 percent of its elastic modulus E_s. There, the yield tensile strength and ultimate tensile strength of steel are f_y and f_{su}, while ε_y and ε_{su} are respectively the yield strain and maximum steel strain.

In the proposed model, the loss of corroded steel is represented simply by reducing the reinforcement cross-section area based on the weight loss from the experimental test. The following equations can calculate the cross-sectional area of the corroded reinforcing steel rebar:

$$A_s = \frac{\pi D^2}{4}\left(1 - \frac{c}{100}\right), \tag{7}$$

$$c = \frac{W_o - W_C}{W_o} * 100, \tag{8}$$

where W_o and W_C are the weight of the sound and corroded reinforcements, *c* represents the degree of corrosion.

Finally, the steel – concrete bond constitutive model was proposed. The amount of steel corrosion and the confinement of the reinforced concrete as indicated by the existence of stirrups are the two main factors that have tremendous effects on the bond stress-slip relationship. There is agreement on its well-defined pattern at the pre-cracking point where the bond strength initially increased with the amount of corrosion and then decreased significantly as the longitudinal corrosion cracking formed along the steel reinforcement. However, for the general design of concrete covers and stirrup quantities, bond failure in RC structures that have corroded steel rebars is often seen by the splitting mechanism. Therefore, for the deteriorated bond between steel and concrete, the residual bond stress-slip curve as proposed by Kallias et al. [12] and Maaddawy et al. [33] is used herein, and the bond stress-slip relationship in CEB-FIP Model Code [31] is used to model the good bond as shown in Fig. 3(c).

$$U_{\max,D} = R\left[0.55 + 0.24\left(c/d_b\right)\right]\sqrt{f_c} + 0.191\left(A_{st} f_{yt}/S_s d_b\right), \tag{9}$$

$$R = A_1 + A_2 m_L, \tag{10}$$

where $U_{\max,D}$ is the residual bond strength, which can be determined by Eq. (9), with *c* being the concrete cover, d_b being the diameter of the longitudinal rebar, A_{st} being the cross-section area of the stirrup, f_{yt} being the yield strength of the stirrup, S_s being the stirrup spacing. R is the factor accountable for the residual contribution of concrete towards the bond strength as a function (Eq. (10)) of A_1 = 1.079 and A_2 = –0.0123 with the corrosion current density i_{corr} (mA/cm²) = 0.35 [33], and m_L is the amount of steel weight loss in percentage. Eq. (9) consists of two different terms: concrete and stirrup contributions to the bond strength are related to the first and second terms, respectively. The effectiveness of this equation is that the level of confinement can be varied with the changes in the stirrup spacing and concrete compressive strength for different specimens. The proposed model of bond deterioration model is validated in the numerical studies of Saether et al. [34]. Otherwise, apart from the empirical models that have been proposed [35–40], the advantages of this bond strength model enable simulating the reduction in confinement and then bond strength of the RC beams without stirrups, including its ability to predict the experimentally observed increase of bond strength for a low degree of corrosion, e.g., the case of tested beams in group C3.

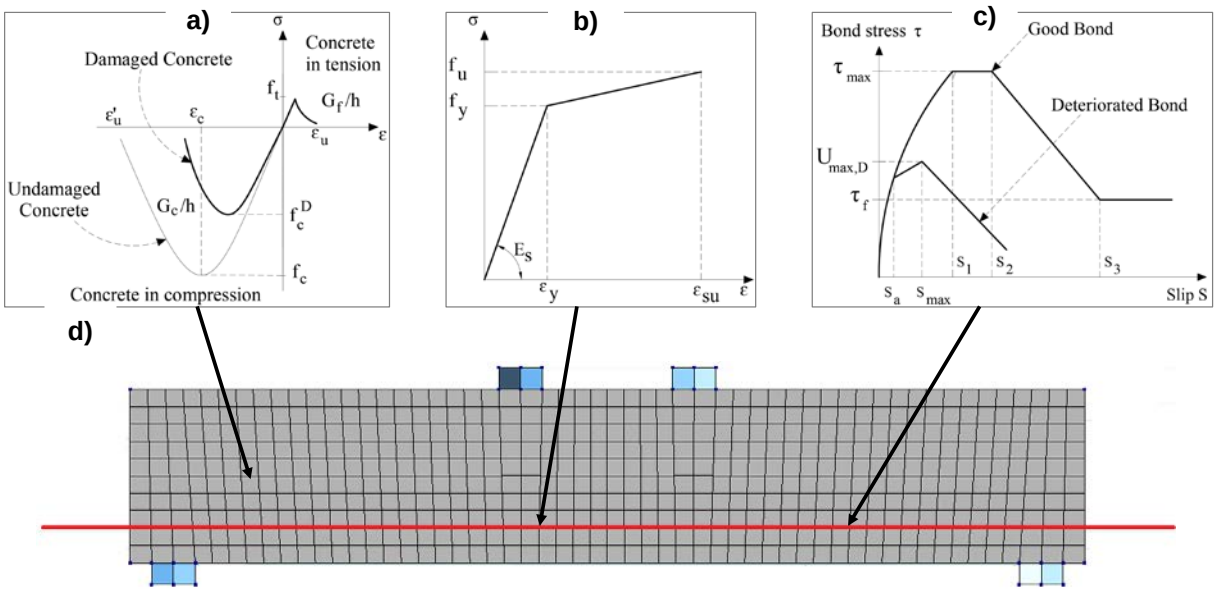

Figure 3. Constitutive models for (a) concrete in compression and tension, (b) steel, (c) bond stress-slip law, (d) mesh discretization of the beam and support conditions.

The concrete is modeled with an element mesh of 20×20×20 mm using a 20-node hexahedron solid element, as illustrated in Fig. 3(d). The compressive strength of concrete is assigned to be 20 MPa on cylinder corresponding to the value obtained from the compression test. Meanwhile, the residual compressive strength of damaged concrete in the target corrosion areas is calculated by Eq. (2) and reduced from 19.2 to 17.8 MPa when increasing the corrosion degree of longitudinal reinforcement from 3 % to 5 %. Moreover, the tensile strength of damaged concrete has remained the identical value as the undamaged concrete at 2.4 MPa. Lastly, the modulus of elasticity for damaged and undamaged concretes shown in Table 3 are calculated by the compressive strength using the formula proposed in CEB-FIP Model Code [31].

In DIANA FEA software, the steel reinforcement is modeled as bond-slip reinforcement. A line-solid interface element has been used in order to simulate the influence of bond-slip behavior because it connects slip reinforcement to the continuum element in which the line element is located. The yield and ultimate tensile strengths of steel used are also summarized in Table 3. In the present simulation, the effect of steel corrosion is modeled by reducing the cross-section of the tension reinforcement based on the corrosion degree. For non-corroded beams, the bond strength and slip parameters are selected based on CEB-FIP Model Code [31], such as the maximum bond strength $\tau_{\max}$ = 10.0 MPa, the residual bond strength τ_f = 1.05 MPa, the slips S_1 = S_2 = 0.6 mm and S_3 = 2.5 mm, and the exponent coefficient α = 0.4. For corroded tension reinforcement, in order to model the splitting failure mode of unconfined RC beams without stirrups, S_1 must be taken close to S_2, and the descending branch must be sharp, reducing the value of S_3, and considering τ_f close to zero. The deteriorated bond curve, as illustrated in

Fig. 3(c), is applied, then the residual bond strength is calculated by Eq. (9) as given in Table 3. In the simulated model of beam C3 and C4, the bond strength enhancement as seen in experiments will be taken into consideration by increasing about 25 % to beam C0.

Table 3. Mechanical properties of materials for modeling tested RC beams.

Beam notation	C0	C3	C4	C5
Residual compressive strength of damaged concrete (MPa)	20	19.2	18.9	17.8
Residual tensile strength of concrete (MPa)	2.4	2.4	2.4	2.4
Young's modulus of concrete (MPa)	25760	25510	25420	25070
Yield tensile strength of steel (MPa)	328.5	328.5	328.5	328.5
Ultimate tensile strength of steel (MPa)	528.8	528.8	528.8	528.8
Elastic modulus of steel (GPa)	210	210	210	210
Maximum bond strength (MPa)	10	12.5	8	2

3. Results and Discussion

3.1. Experimental results of shear behavior

A total of eight experimental beams were fabricated and tested in the laboratory. Six beams belong to groups C3, C4, and C5 were subjected to accelerated corrosion, and the remaining two beams of group C0 were retained as non-corroded control beams. All beams were without compression and transverse shear reinforcement. Test variables included the different degrees of corrosion of 0 %, 3.13 %, 4.1 %, and 4.93 % on average. The shear responses of the experimental beams are shown in Fig. 4. For the control beams, three distinct phases will characterize the load – deflection response, as follows: (i) the first phase represents the action of an un-cracked beam with a gross inertia moment; (ii) the second phase represents the first shear crack with a reduced inertia moment; (iii) the third phase is the post-peak phase after failure. In the control beams C0-1 and C0-2, the first crack was observed at the load of approximately 7.5 kN, and shear failure occurred at the ultimate load of 34.8 and 35.1 kN, respectively. The corroded beams belong to groups C3 and C4 exhibited shear behavior similar to that of the control beams. However, in the case of the beams C3-1 and C3-2 having the target corrosion degree of 3.16 % and 3.10 %, respectively, the shear strength was increased by approximately 7 % (37.5 kN versus 35 kN on average) while in the case of the beams C4-1 and C4-2 the maximum capacity is nearly equal to the result of the control beams in group C0. These results can be explained that the bond stress between steel and concrete increases in the experimental beams having the corrosion degree smaller than 4 % regardless of the corrosion cracks that occurred along the longitudinal reinforcement that is mentioned in the literature [10, 20, 41].

In addition, the beams C5-1 and C5-2 that were attacked by more severe corrosion had lower overall initial stiffness than the other tested beam specimens. There were no apparent shear cracks but the flexural cracks in the beam web during the test. It is also stated that the width of the splitting cracks gradually increased with load increase after the splitting cracking formed along the longitudinal reinforcing rebars, and failure occurred at 32.5 kN and 30.2 kN corresponding to a decrease of 10 % in comparison with those of the control beams. This is because the bond-loss between reinforcement and concrete dominates the failure mechanism of these corroded RC beams as the corrosion degree increases before sufficient tensile forces are developed in the tension reinforcement to resist the in-plane bending moment.

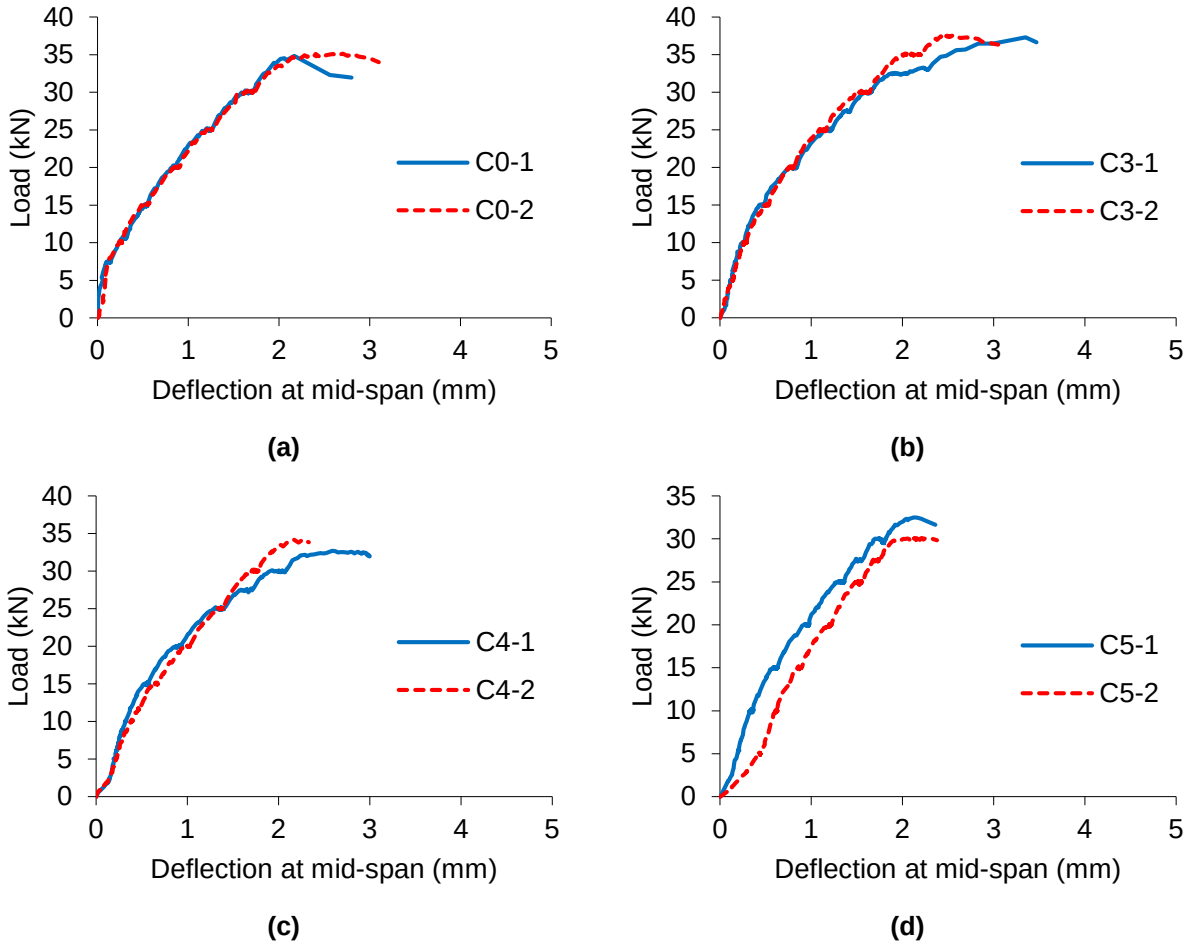

Figure 4. Load – deflection curves of the experimental beams: (a) group C0, (b) group C3, (c) group C4, (d) group C5.

Table 4 synthesizes the main results obtained using the four-point loading test for each experimental beam, characterized by the corrosion degree of longitudinal reinforcement, ultimate load, and failure mode. For each test group, the average value of the ultimate load is calculated in order to compare the shear strength and failure modes between the beams with different degrees of corrosion.

Table 4. Summary of test results.

Beam notation	Degree of corrosion *c* (%)	Ultimate load *P* (kN)	Average ultimate load (kN)	Failure mode
C0-1	0	34.8	35.0	Diagonal tension failure
C0-2	0	35.1		Diagonal tension failure
C3-1	3.16	37.3	37.5	Diagonal tension failure
C3-2	3.10	37.6		Diagonal tension failure
C4-1	4.27	35.4	34.8	Diagonal tension failure
C4-2	3.94	34.2		Diagonal tension failure
C5-1	4.99	32.5	31.3	Shear tension failure
C5-2	4.87	30.2		Shear tension failure

3.2. FEM results of shear behavior

Fig. 5 illustrates the comparison between the results of tested beams by experimental and numerical approaches. It is confirmed that the simulation by modifying the constitutive materials shown in section 3 is capable of modeling the response of corroded RC beams with reasonable accuracy between the two approaches results for the load – deflection curves of the control beam C0 and three corroded beams C3, C4, C5. FE model can predict the ultimate flexural strength of tested beams C0, C3, and C5 with good accuracy. The beam C4 with a 4 % degree of corrosion in stirrups has the least reduction in load-carrying capacity, 34.2 kN in the test versus 31.5 kN in FEM. The ultimate load of the beam C5 in the test was 30.2 kN compared with approximately 30.5 kN at the same deflection of FEM results.

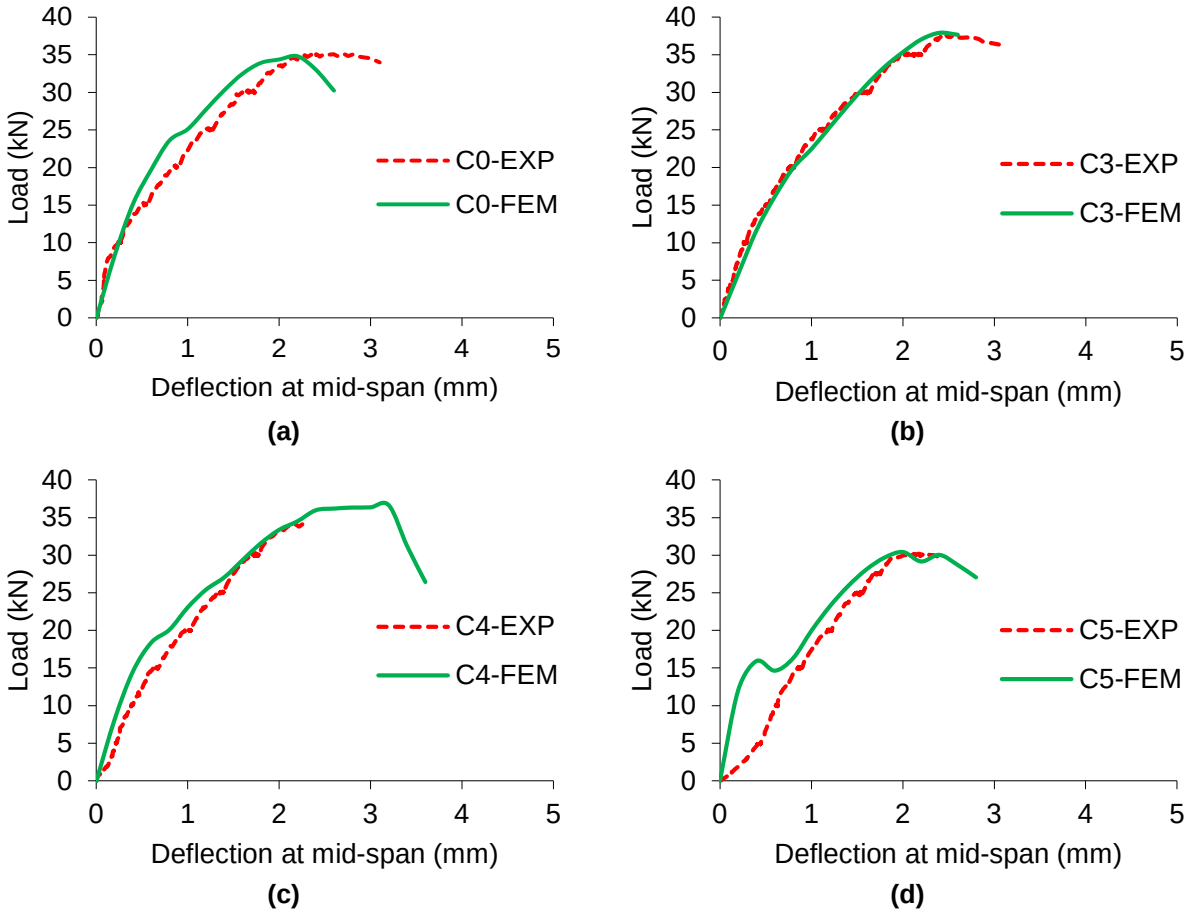

Figure 5. Load – deflection curves of corroded beams using experiment and FEM.

Due to the increasing corrosion degree of tension reinforcement of eight tested beams, the cross-sectional areas of the tension reinforcement decreased, and the concrete cover cracked, leading to a reduction of the effective cross-section. The shear strength of corroded RC beams is considerably low in all cases. The shear strength dropped rapidly after the peak load, and a small displacement increment caused a large decrease in shear strength, which is a characteristic of the shear failure mode. Small amounts of steel corrosion, prior to the development of visible concrete cracking, tend to cause an increase of bond strength between the steel rebars and concrete. Bond strength begins to deteriorate with the formation of corrosion cracking in concrete, typically along the reinforcement length.

As mentioned in the literature review, the shear strength of concrete beams without shear reinforcement is determined by the shear strength of the concrete compressive zone, the shear force due to dowel action, aggregate interlock, and bond strength with efficient anchorage condition. In the case of group C3, by sensitively increasing the maximum bond strength from 10 MPa in the case of a good bond to 12.5 MPa (cf. Table 3), the maximum capacity obtained of beam C3 from the test can be simulated by a numerical approach without considering the bond enhancement of tension reinforcement due to the dowel action as it is shown in Fig. 5.

Otherwise, in the case of group C5, FEM simulation shared the same maximum capacity as reported from the test, which is around 10 % less than those of the non-corroded beam. The differences in the initial stiffness between experimental and numerical approaches can be seen. In the test, due to the significant amount of crack forming along the tension reinforcement from the accelerated corrosion stage, the tested C5 beam shared the significantly larger deflection at 10 kN load, which indicates the lower initial stiffness than other tested beams. On the other hand, by using the FEM simulation, the maximum bond strength was decreased from 10 MPa in the case of a good bond to around 2 MPa (cf. Table 3). The performance of the simulated beam C5 is similar to beam specimens during the elastic stage. The corresponding load later shows a slight decrease before rising significantly and shared the same value at the failure stage as it is given in the experimental test. This is because the loss in bond strength between steel and concrete only has a contribution to the structural performance of the beam after the first crack occurrence, or the tensile stress in concrete surpasses its tensile strength.

In general, the results of corroded beams in FEM simulation showed the sensitive responses to the selection of the model of bond strength reduction with the corresponding parameters assigned in DIANA. The lack of a formulation for the bond strength in simulation for corroded steel rebars with varying diameters

in tension reinforcement is a barrier against accurate estimation for the ductility of FEM simulated and tested beams. It can be seen by the differences in deflection at the failure stage of both methods. There was a noticeable difference in the stiffness of the FE model comparing with the experimental beams, and it can be ascribed to initial cracking in concrete before loading due to the corrosion of steel rebars when the simulated beams were considered uncracked at the onset of the FE analysis.

(a) **(b)**

Figure 6. Failure modes of tested beams: (a) Diagonal tension failure, (b) Shear tension failure.

The crack strain distribution obtained from FE analysis was also compared with the experimental results as shown in Fig. 6 for both types of failure modes (cf. Table 4) to confirm the applicability and accuracy of the model. As stated previously, all tested specimens exhibited shear dominant failure, and cracks mostly occurred in the zone of the beam with the maximum shear load. Fig. 7 shows the maps of concrete cracks due to loading for each tested beam, which is identified by the test and the FE model. The cracking patterns of the control beams and corroded beams are consisting of corrosion cracks marked red and loading cracks (i.e. flexural cracks in loading and shear cracks at failure). For the sample groups C0, C3, and C4, the corrosion cracks propagated for a limited length along longitudinal reinforcement, while they propagated for the total length of the corroded beams in group C5. As it is illustrated, FEM results can represent the crack pattern of the tested beams with a good correlation.

For the control beams C0-1 and C0-2, they showed typical diagonal tension failure mode, which is a sudden failure of concrete in shear. In group C3, the development of vertical cracks (flexural cracks) at the bottom of the beam due to flexural tensile stress has led to diagonal tension failure. If the load on the beam increases, as it propagates from the support point of the beam towards the loading point, these cracks expand both in width and length and bend in a diagonal direction. The beams in groups C3 and C4 exhibited a similar failure mode and shear crack pattern to those of the reference specimen. The corroded beams C5-1 and C5-2, which have higher corrosion degrees, showed a different failure mode. In particular, as the degree of corrosion reached 5 %, beam C5-2 had a shear tension failure at the final stage and illustrated a tendency that the width of the splitting cracks caused by corrosion increased significantly as the external load increased. Moreover, the diagonal cracks propagate horizontally along the rebars, it is mainly because of inadequate anchorage of the longitudinal rebars, and the specimen failed abruptly with the occurrence of the nearly vertical critical shear cracks at the maximum load-carrying capacity. While it should be noted that smeared cracking approach provides a rough estimation about stress-release resulting from cracking [42], the present finite element analysis exhibited a similar cracking pattern.

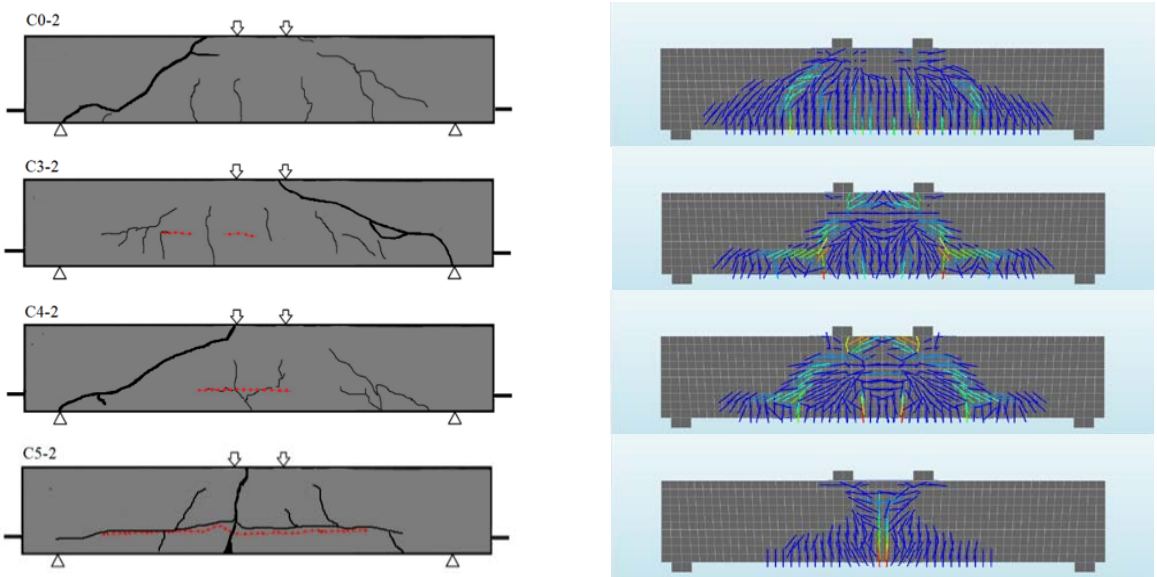

Figure 7. Cracking patterns at the failure of the beams using test and FEM.

3.3. Parametric study

According to the current design codes such as CEB-FIP Model Code 2010 [31] and ACI 318-19 [43], the beams that have the shear span-effective depth ratio (a/d) smaller than 2.0 are considered as deep beams. In general, deep beams can sustain high shear strength because of the tie-arched mechanism that distributes the load directly to the support through concrete compressive struts. This type of beam usually fails by shear compression failure, which occurs at the tip of the shear crack when the compressive strength of the concrete is exceeded in the compression area. Meanwhile, the beams with the a/d ratios greater than 2.0 are slender beams. In slender beams, the beam mechanism plays a more important role. This is because the considerably increasing distance between the loading point and the support has deteriorated the tied-arch mechanism. After the failure of the beam mechanism, the diagonal cracks propagate rapidly to the loading point with the sudden breakdown of aggregate interlock, which causes diagonal tension failure. To examine the FE model capability in simulating the different behavior associated with beam and tie-arched mechanisms, the tested beam C4 without shear reinforcement and shear span-to-depth ratios ranging from 1.0 to 6.0 are considered as illustrated in Fig. 8.

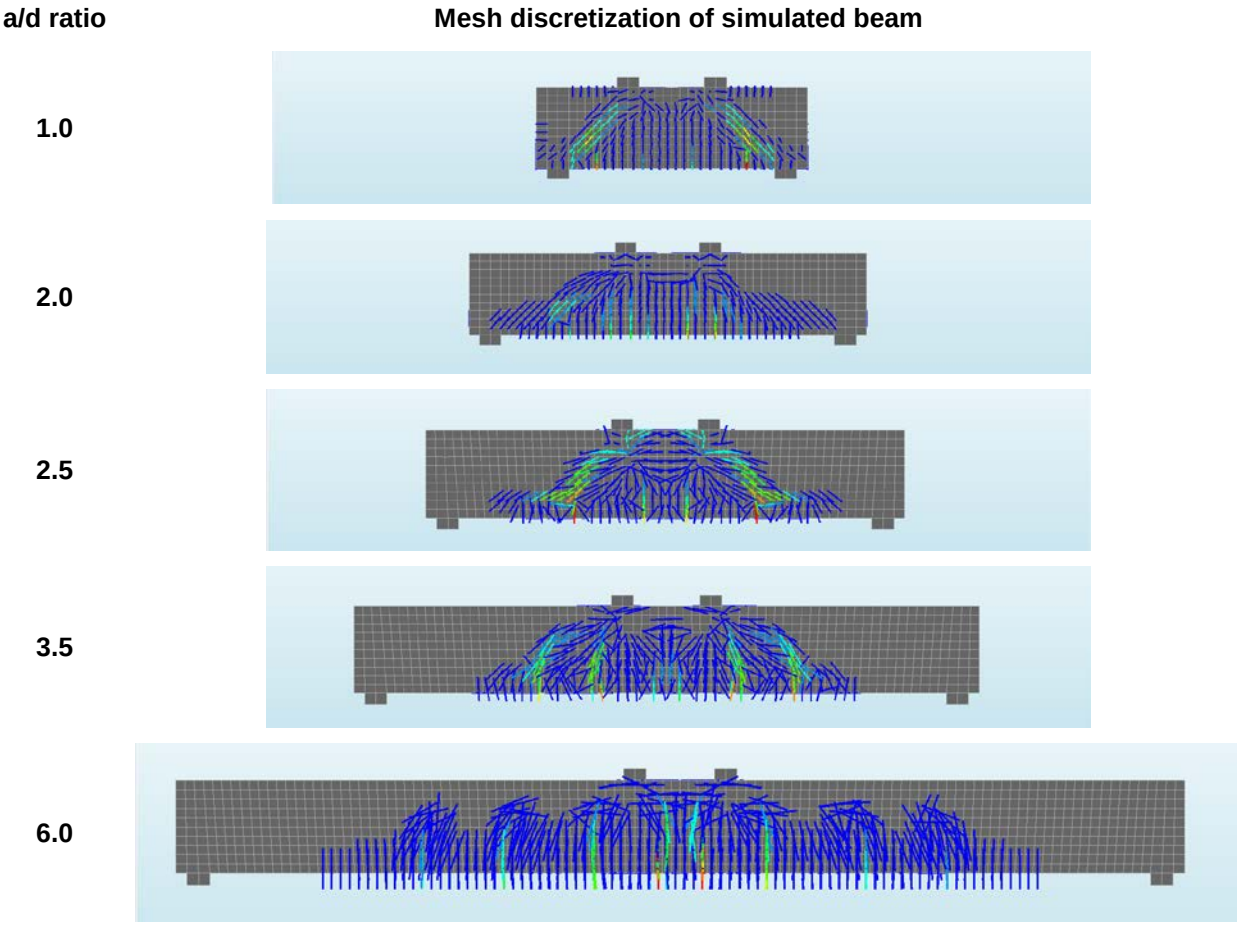

Figure 8. Crack strain distribution at the failure of simulated beams with different a/d ratios.

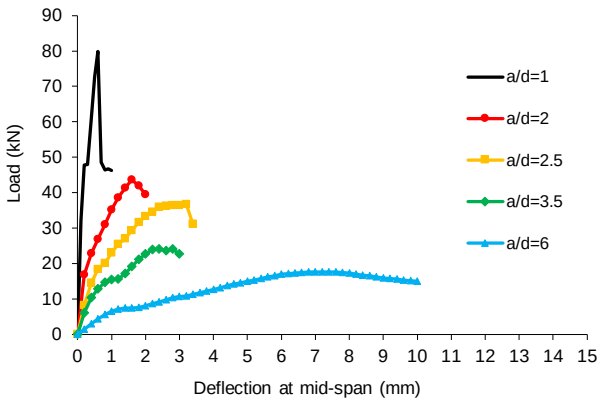

Figure 9. Load - deflection curves of simulated corroded beams with different shear span-to-depth ratios.

Fig. 8 shows the crack strain distribution at failure. The presence of a well-defined inclined strut from load point to support is evident for the a/d ratio equals to 1.0. The numerical results show that the higher strains are localized below the line connecting the load and support points. On the other hand, for the a/d higher ratios of 2.0, 2.5, 3.5, the beam action is shown by the horizontal compression chord at the top of the beam and the wide inclined compression field in the web. The failures observed are due to crack propagation which is the splitting crack starting parallel to the reinforcement, propagating diagonally across the web, and finally splitting the top concrete cover. Lastly, the crack strain distribution at the failure stage of a beam with the a/d ratio equals to 6 was observed, several vertical cracks appeared around the mid-span rather than the formation of diagonal crack, which indicates the flexural failure. Fig. 9 shows the load – deflection curves of the simulated beams having the a/d ratio ranging from 1.0 to 6.0. It indicates that the shear span-to-depth ratio is a significant factor affecting the shear strength of all simulated beams. This is because the load-carrying capacity of the beams decreased considerably with increasing the a/d ratio. The maximum shear strength of the simulated beam having the a/d ratio equals to 1 is approximately 100 %, 166 %, and 220 % larger than beams having a/d ratio equal to 2.0, 2.5, and 3.0, respectively. When a/d equals to 6, the failure mode shifted from shear failure to flexural failure having the maximum capacity of around one-third of the beam with a/d equal to 1.

4. Conclusions

In this paper, an experimental study and a 3D non-linear FE model simulation are carried out to assess the structural performance of a series of eight RC beams without shear reinforcement damaged by varying degrees of steel corrosion. The results of FE analyses were compared to the experimental results to investigate the accuracy of the numerical approach. Key parameters affecting the shear strength of tested beams are identified. These include the influence of compressive strength of concrete, impaired bond performance (due to corrosion in the tension reinforcement), and reduced cross-section area of tension reinforcement. The parametric study of different shear span-to-depth ratios was also conducted to examine the FE model capability in simulating the different behavior associated with beam and tie-arched mechanisms. The main conclusions are drawn as follows:

1. The tension reinforcement corrosion has an overall adverse effect on the shear performance of RC beams. In the corroded beams where the tension reinforcement subjected to corrosion degree smaller than 4 %, specimens showed about 7 % increase of shear strength, compared with control beams. Even when the beams were subjected to 4 % degree of corrosion in tension reinforcement, the maximum shear capacity obtained still remained the same as of the control beams because of the increase in bond stress between tension reinforcement and concrete regardless of the formation of crack openings from accelerated corrosion process.

2. The main cause for the loss of shear strength in corroded RC beams without stirrups is due to the impaired bond. While the structural behavior of experimental beams can be simulated by reducing the bond strength values, this indicates that the deterioration of bond behavior has a significant contribution to the structural performance of corroded RC beams even with the relatively small degree of corrosion, which is around 5 %.

3. The adoption of the extended finite element method has the ability to predict the load – deflection response, cracking pattern of corroded RC beams without shear reinforcement. In the case of the beams with the corrosion degree smaller than 4 %, loss of steel cross-sectional area and associated compressive strength of concrete loss in the finite element analyses were found to have a significant influence.

4. The accuracy of the FE model is validated in the parametric study. The use of such numerical models can not only serve as a tool for assessing existing structures that are designed and constructed without shear reinforcement and also as a complementary tool for planning and optimization of the experimental studies by establishing the preliminary parameter sensitivity.

References

1. Castel, A., François, R., Arliguie, G. Mechanical behaviour of corroded reinforced concrete beams – Part 1: Experimental study of corroded beams. Materials and Structures. 2000. 33. Pp. 539–544.
2. Torres-Acosta, A.A., Fabela-Gallegos, M.J., Munoz-Noval, A., Vázquez-Vega, D., Hernandez-Jimenez, J.R., Martinez-Madrid, M. Influence of corrosion on the structural stiffness of reinforced concrete beams. Corrosion. 2004. 60(9). Pp. 862–872.
3. Torres-Acosta, A.A., Navarro-Gutierrez, S., Terán-Guillén, J. Residual flexure capacity of corroded reinforced concrete beams. Engineering Structures. 2007. 29(6). Pp. 1145–1152.
4. Almusallam, A.A., Al-Gahtani, A.S., Aziz, A.R., Dakhil, F.H., Rasheeduzzafar. Effect of reinforcement corrosion on flexural behavior of concrete slabs. Journal of Materials in Civil Engineering. 1996. 8(3). Pp. 123–127.
5. Rodriguez, J., Ortega, L.M., Casal, J. Load carrying capacity of concrete structures with corroded reinforcement. Construction and Building Materials. 1997. 11(4). Pp. 239–248.
6. Soltani, M., Safiey, A., Brennan, A. A state-of-the-art review of bending and shear behaviors of corrosion-damaged reinforced concrete beams. ACI Structural Journal. 2019. 116(3). Pp. 53–64.

7. Zhu, W., François, R., Fang, Q., Zhang, D. Influence of long-term chloride diffusion in concrete and the resulting corrosion of reinforcement on the serviceability of RC beams. Cement and Concrete Composites. 2016. 71. Pp. 144–152.
8. Xu, S., Zhang, Z., Li, R., Qiu, B. Experimental study on the shear behavior of RC beams with corroded stirrups. Journal of Advanced Concrete Technology. 2017. 15(4). Pp. 178–189.
9. Higgins, C., Farrow, W.C.III. Tests of reinforced concrete beams with corrosion-damaged stirrups. ACI Structural Journal. 2006. 103(1). Pp. 133–141.
10. Lachemi, M., Al-Bayati, N., Sahmaran, M., Anil, O. The effect of corrosion on shear behavior of reinforced self-consolidating concrete beams. Engineering Structures. 2014. 79. Pp. 1–12.
11. El-Sayed, A.K., Hussain, R.R., Shuraim, A.B. Influence of stirrup corrosion on shear strength of reinforced concrete slender beams. ACI Structural Journal. 2016. 113(6). Pp. 1223–1232.
12. Kallias, A.N., Imran Rafiq, M. Finite element investigation of the structural response of corroded RC beams. Engineering Structures. 2010. 32(9). Pp. 2984–2994.
13. Biswas, R.K., Iwanami, M., Chijiwa, N., Uno, K. Effect of non-uniform rebar corrosion on structural performance of RC structures: A numerical and experimental investigation. Construction and Building Materials. 2020. 230. 116908.
14. Blomfors, M., Lundgren, K., Zandi, K. Incorporation of pre-existing longitudinal cracks in finite element analyses of corroded reinforced concrete beams failing in anchorage. Structure and Infrastructure Engineering. 2020. 1–17.
15. Coronelli, D., Gambarova, P. Structural assessment of corroded reinforced concrete beams: modeling guidelines. Journal of Structural Engineering. 2004. 130(8). Pp. 1214–1224.
16. Coronelli, D., Mulas, M.G. Modeling of shear behavior in reinforced concrete beams. ACI Structural Journal. 2006. 103(3). Pp. 372–382.
17. Huang, L., Ye, H., Jin, X., Jin, N., Xu, Z. Corrosion-induced shear performance degradation of reinforced concrete beams. Construction and Building Materials. 2020. 248. 118668.
18. Nakamura, H., Iwamoto, T., Fu, L., Yamamoto, Y., Miura, T., Gedik, Y.H. Shear resistance mechanism evaluation of RC beams based on arch and beam actions. Journal of Advanced Concrete Technology. 2018. 16(11). Pp. 563–576.
19. Toongoenthong, K., Maekawa, K. Interaction of pre-induced damages along main reinforcement and diagonal shear in RC members. Journal of Advanced Concrete Technology. 2004. 2(3). Pp. 431–443.
20. Han, S., Lee, D., Yi, S., Kim, K.S. Experimental shear tests of reinforced concrete beams with corroded longitudinal reinforcement. Structural Concrete. 2020. 21(5). Pp. 1763–1776.
21. Tan, N.N., Kien, N.T. An experimental study on the shear capacity of corroded RC beams without shear Reinforcement. Journal of Science and Technology in Civil Engineering. NUCE 2021. 15(1). Pp. 55–66.
22. Maekawa, K., Hasegawa, T. The state-of-the-art on constitutive laws of concrete. Concrete Journal. 1994. 32(5). Pp. 13–22.
23. Maekawa, K., Pimanmas, A., Okamura, H. Nonlinear mechanics of reinforced concrete. Spon Press, London, 2003.
24. Shayanfar, M.A., Barkhordari, M.A., Ghanooni-Bagha, M. Effect of longitudinal rebar corrosion on the compressive strength reduction of concrete in reinforced concrete structure. Advances in Structural Engineering. 2016. 19(6). 897–907.
25. Lim, S., Akiyama, M., Frangopol, D.M. Assessment of the structural performance of corrosion-affected RC members based on experimental study and probabilistic modeling. Engineering Structures. 2016. 127. Pp. 189–205.
26. TNO. DIANA 9.1 User's manual. TNO Building and Construction Research. Delft, 2005.
27. Nakamura, H., Higai, T. Compressive fracture energy and fracture zone length of concrete. In: Shing P., Tanabe T., editors. Modelling of inelastic behaviour of RC structures under seismic loads. American Society of Civil Engineers. 2001. Pp. 471–487.
28. Cape, M. Residual service-life assessment of existing R/C structures. MS thesis, Chalmers Univ. of Technology (Goteborg, Sweden) and Milan Univ. of Technology (Italy, Erasmus Program), 1999.
29. Molina, F.J., Alonso, C., Andrade, C. Cover cracking as a function of rebar corrosion: Part 2 – Numerical model. Materials and Structures. 1993. 26. 532–548.
30. Val, D.V. Deterioration of strength of RC beams due to corrosion and its influence on beam reliability. ASCE Journal of Structural Engineering. 2007. 133(9). Pp. 1297–1306.
31. CEB-FIP Model Code. fib model code for concrete structures 2010. fib, Berlin, Germany.
32. Du, Y.G., Clark, L.A., Chan, A.H.C. Residual capacity of corroded reinforcing bars. Magazine of Concrete Research. 2005. 57(3). Pp. 135–147.
33. Maaddawy, T.E., Soudki, K., Topper, T. Analytical model to predict nonlinear flexural behaviour of corroded reinforced concrete beams. ACI Structural Journal. 2005. 102(4). Pp. 550–559.
34. Sæther, I., Sand, B. FEM simulation of reinforced concrete beams attacked by corrosion. ACI Structural Journal. 2012. 39(2). Pp. 15–31.
35. Tran, N.L. A new shear model for fibre-reinforced concrete members without shear reinforcement. In: Hordijk D., Luković M. (eds) High Tech Concrete: Where Technology and Engineering Meet. Springer, Cham. DOI: 10.1007/978-3-319-59471-2_86
36. Tran, N.L. A mechanical model for the shear capacity of slender reinforced concrete members without shear reinforcement. Engineering Structures. 2020. 219. 110803.
37. Khan, I., François, R., Castel, A. Experimental and analytical study of corroded shear-critical reinforced concrete beams. Materials and Structures. 2013. 47(9). Pp. 1467–1481.
38. Lu, Z.-H., Li, H., Li, W., Zhao, Y.-G., Dong, W. An empirical model for the shear strength of corroded reinforced concrete beam. Construction and Building Materials. 2018. 188. Pp. 1234–1248.
39. Krishan, A., Narkevich, M., Sagadatov, A., Rimshin, V. The strength of short compressed concrete elements in a fiberglass shell. Magazine of Civil Engineering. 2020. 94(2). Pp. 3–10.
40. Kim, H.-G., Jeong, C.-Y., Kim, M.-J., Lee, Y.-J., Park, J.-H., Kim, K.-H. Prediction of shear strength of reinforced concrete beams without shear reinforcement considering bond action of longitudinal reinforcements. Advances in Structural Engineering. 2017. 21(1). Pp. 30–45.
41. Lushnikova, V.Y., Tamrazyan, A.G. The effect of reinforcement corrosion on the adhesion between reinforcement and concrete. Magazine of Civil Engineering. 2018. 4(80). Pp. 128–137.

42. An, X., Maekawa, K., Okamura, H. Numerical simulation of size effect in shear strength of RC beams. Journal of Materials, Concrete Structures and Pavement. JSCE 1997. 35. Pp. 297–316.
43. ACI 318-19. Building Code Requirements for Structural Concrete and Commentary. American Concrete Institute. 2019.

Contacts:

Ngoc Tan Nguyen, *PhD*
ORCID: https://orcid.org/0000-0002-4841-0653
E-mail: tannn@huce.edu.vn

Trung Kien Nguyen
ORCID: https://orcid.org/0000-0002-3108-6463
E-mail: kiennt2@huce.edu.vn

Hoang Giang Nguyen, *PhD*
ORCID: https://orcid.org/0000-0001-7505-2233
E-mail: giangnh@huce.edu.vn

Received 07.03.2021. Approved after reviewing 19.07.2021. Accepted 19.07.2021.